

Simulation study for the formation of alkaline efflorescence on bauxite residue disposal areas following the phosphogypsum addition

by Wu, Y., Li, M., Fu, D., Santini, T.C., Jiang, J., Hartley, W. and Xue, S.

Copyright, publisher and additional Information: This is the author accepted manuscript. The final published version (version of record) is available online via Elsevier.

This version is made available under the CC-BY-ND-NC licence:
<https://creativecommons.org/licenses/by-nc-nd/4.0/legalcode>

Please refer to any applicable terms of use of the publisher

DOI: <https://doi.org/10.1016/j.jclepro.2020.121266>



**Harper Adams
University**

Simulation study for the formation of alkaline efflorescence on bauxite
residue disposal areas following the phosphogypsum addition

Yujun Wu^a, Meng Li^a, Ding Fu^b, Talitha C. Santini^c, Jun Jiang^a, Hartley William^d,
ShengguoXue^{a,*}

a. School of Metallurgy and Environment, Central South University, 932 Lushan South Road,
Changsha, 410083, PR China

b. Business School, Beijing Normal University, 19 Xijiekouwai Street, Beijing, 100875, P.R.
China

c. School of Agriculture and Environment, The University of Western Australia, 35 Stirling
Highway, Crawley, Western Australia 6009, Australia

d. Crop and Environment Sciences Department, Harper Adams University, Newport,
Shropshire, TF10 8NB, United Kingdom

Abstract

Bauxite residue is a solid, highly alkaline byproduct (tailings) generated in the alumina refining process. The process that forms the fine white salt deposits on the surface of bauxite residue following prolonged dry periods, and which also forms on products made from reused residues (sintered bricks, etc.), is known as efflorescence. It not only seriously affects the utilization of bauxite residue in building materials, but also creates potential dust pollution around the BRDAs, which means it would require sustained and intensive resources to manage and transform its alkalinity. Through a laboratory simulation experiment using soil leaching columns, we show that the extent of bauxite residue efflorescence is affected by many factors, including porosity, initial water content, bauxite residue particle size. The main soluble mineral precipitates of efflorescence are Na_2CO_3 and NaHCO_3 . Addition of phosphogypsum, a common amendment to reduce dispersion and promote removal of Na^+ through leaching, shifted the composition of effloresced salts to favor $\text{Na}_2\text{SO}_4 \cdot 10\text{H}_2\text{O}$. SEM and Na K-edge X-ray absorption near-edge structure (XANES)spectroscopy demonstrated that free alkali migrates to the residue surface to precipitate as a uniform agglomerate in the efflorescence process, which also changes the chemical form of Na-containing minerals in the bauxite residue and the mesoscale spatial distribution of Na (soft X-ray scanning transmission microscopy imaging). Free alkali migration with water is the main driver of efflorescence, and this work also demonstrated that phosphogypsum can reduce the

generation of alkaline efflorescence for ameliorating alkaline dust pollution from bauxite residue.

Keywords

Bauxite residues, efflorescence, phosphogypsum, alkaline substance, alkalinity migration

1. Introduction

Bauxite residue is the solid byproduct (tailings) generated after extracting alumina from bauxite via the Bayer process, sintering process, and combined Bayer-sintering process. The current global stock of bauxite residue is estimated at 4.6 billion tons, and the annual increase in bauxite residue in China alone is estimated at 200 million tons, mainly deposited by dry stacking (solids content 50-65 wt.%) (Xue et al., 2019a). Bauxite residue has a high alkali content, which creates serious challenges for storage and utilization (Wen et al., 2016; Xue et al., 2016; Yoon et al., 2019). The substantial amount of bauxite residue in bauxite residue disposal areas (BRDAs) not only occupies large areas of otherwise productive land (Sofra and Boger, 2002; Liu et al., 2009; Xue et al., 2020), but can also be a source of fugitive dust emissions which result in environmental and air pollution. These dust emissions are exacerbated by high winds and/or low rainfall (Klauber et al., 2013; Kong et al., 2017a; Xu et al., 2018). Bauxite residue has a fine particle size, concentrated in the range of 2 to 100 μm (Grafe et al., 2011; Zhu et al., 2017), and these fine bauxite residue particles (including minerals such as hematite (Fe_2O_3), calcite (CaCO_3), and desilication product minerals such as hydrogarnet ($(\text{Ca}_3\text{Al}_2(\text{SiO}_4)_x(\text{OH})_{12-4x})$ and cancrinite ($\text{Na}_8\text{Al}_6\text{Si}_6\text{O}_{24}(\text{CO}_3)(\text{H}_2\text{O})_2$) contribute to dust emissions from BRDAs (Gelencser et al., 2011). Much of the fugitive dust emissions also comprise salts precipitated at the residue surface through efflorescence. These salts typically appear as a layer of white material on the bauxite residue surface after deposition in BRDAs, through capillary rise of dissolved alkali in pore water and evaporation of water at the residue surface (Klauber et al., 2013). Sodium ions can't form stable hydration layers and can't be coordinated with negatively charged surfaces, which results in the particles of fresh bauxite residue disaggregating and hence a crusted surface forms as Na eventually

precipitates out as soda ash (trona and nahcolite) (Kong et al., 2017a). The soluble alkaline substances in bauxite residue diffuse to its surface, and react with CO₂ in the atmosphere, to form white monohydrate carbonate deposits on the surface. Higgins et al. (2018) found that carbonation of bauxite residue leachate is an important component of passive treatments and neutralization. The rate of in-gassing and diffusion of CO₂ controls the depth to which this process can act within bauxite residue. Bray et al. (2018) demonstrated that atmospheric CO₂ in-gassing appears to extend ~20 cm below the surface. Hence, efflorescence is partially controlled by the balance between CO₂ infiltration from the atmosphere. The effloresced minerals include strongly alkaline (often sodium-based) salts such as sodium carbonate (soda ash; Na₂CO₃), trona (Na₂CO₃·NaHCO₃·2H₂O), and nahcolite (NaHCO₃) (Klauber et al., 2013), which can cause impacts to the surrounding environment and human health. Efflorescence also negatively affects the utilization prospects for bauxite residue in construction applications. Delamination and crumbling due to efflorescence of alkali salts impacts visual appearance of building materials using bauxite residue as well as decreasing the longevity and strength of the material (Wang et al., 2018; Huang et al., 2014).

In warmer climates, unregulated bauxite residue disposal areas can be a significant source of fugitive dust emissions, which result in the health hazard posed by the inhalation of caustic compounds. At present, dust control in bauxite residue deposits is primarily achieved by chemical stabilizers or irrigation (water application). Chemical stabilizers are difficult to apply, high cost, temporary in effect, and pose additional issues for energy consumption and environmental management (e.g. downstream impacts to groundwater and the tailings themselves) (Indraratna et al., 2013; Rollings et al., 1999; Vinod et al., 2010; Gomes et al., 2016). Polymer stabilizers are an emerging approach technology but have only been tested on residue sand (coarse fraction) (Ding et al., 2019) and are not yet employed at field scale. At present, the most common efflorescence suppression approaches for bauxite residue are pH neutralization (dealkalization; mostly for residues in BRDAs) or sodium stabilization

(mostly for residues reused in building applications). pH neutralization, destroying free alkali, can be achieved by water washing, application of inorganic or organic acids, and other methods such as seawater application (Luo et al., 2017; Johnston et al., 2010; Khaitan et al., 2009; Lehoux et al., 2013; Santini and Peng, 2017; Santini et al., 2015; Smiciklas et al., 2014; Collins et al., 2014). Sodium stabilization refers to the incorporation of previously free sodium into sparingly soluble or insoluble minerals, usually through high temperature treatment such as sintering (Mishra et al., 2002; Hong and Glasser, 2002; Wieszlawski, 1999).

There is currently a gap in knowledge linking the nature and formation mechanism of fugitive dusts from efflorescence in a BRDA to the development and implementation of a tailored dust/efflorescence suppression approach that targets the root cause(s) of efflorescence in bauxite residue. Understanding the chemistry behind the efflorescence process gives the best opportunity to target appropriate lower cost mitigation strategies, rather than implementing a suite of traditional binders and stabilizers developed for other dust sources. Application of phosphogypsum (a residue produced during P fertilizer production) may offer one such opportunity to target the root cause(s) of efflorescence by simultaneously decreasing free alkali and the high sodicity of bauxite residue (Shi et al., 2017; Jones et al., 2011; Sharma et al., 2004; Li et al., 2019). Most of the focus to date relating to (phospho-) gypsum application in residue has been focused on amelioration of residue properties to promote vegetation establishment and growth (Bray et al., 2018; Courtney and Timpson, 2004; Courtney and Harrington, 2012; Courtney et al., 2014; Courtney and Xue, 2019). Although the effects of gypsum in decreasing pH and replacing free and exchangeable Na^+ with Ca^{2+} have been consistently noted in these studies, no study to date has specifically investigated the role of phosphogypsum in producing efflorescence and reducing alkaline dust generation from bauxite residues.

This study is therefore focused on understanding the key solutes and transport processes underpinning efflorescence in bauxite residue, with and without

phosphogypsum application, as a commonly in-situ remediation amendment for application in BRDAs. Through a laboratory soil column experiment, we investigated: 1) the chemical and mineral composition of effloresced salts at bauxite residue surfaces; 2) the process and key factors controlling the composition and quantity of effloresced salts; 3) the role of phosphogypsum application in reducing the composition and quantity of alkaline effloresced salts. Based on results from this study, we provide recommendations for the management of efflorescence in BRDAs and the large-scale utilization of bauxite residue resources in building and construction materials in the future.

2. Material and methods

2.1 Samples

The bauxite residue used in the experiment was taken from a BRDA in Guangxi, China (23°18'N, 107°31'E). Samples were fresh bauxite residues (deposited less than one month and untreated), randomly sampled in the BRDA, evenly mixed to create one homogeneous sample, and then dried at room temperature to constant weight. Gravel (fragments > 2 mm in diameter) was removed by hand and the residue was sieved to <0.84 mm (20 mesh). The initial geochemical and physical properties of the bauxite residue used in the experiment are shown in Table 1.

2.2 Experimental design and apparatus

A simulation experiment using a laboratory soil column was conducted to study the process of efflorescence. The effect of experimental scale on the simulation results, and the difference between laboratory conditions and field conditions, was also considered. The column comprised a polymethyl methacrylate (PMMA) cylinder (height 95 cm; inner diameter 12.6 cm), into which six sampling holes (diameter 2 cm) spaced 10 cm apart from each other along the longitudinal axis were drilled (Fig.1). The water collector was positioned underneath the column, and the water dripper (attached to a peristaltic pump) was positioned above the column.

Two soil columns were established for the experiment, each containing a layer of gauze (nylon, 0.45 mm) placed on the porous baffle (stainless steel) at the bottom of the soil column, then a 15 cm layer of quartz sand. Column 1 (C1) was then filled with 80 cm of bauxite residue to simulate unamended BRDAs; whereas column 2 (C2) was filled with 55 cm of bauxite residue at the bottom and then 25 cm of bauxite residue at the top amended with 2% (wt.%) phosphogypsum to simulate phosphogypsum-amended BRDAs. After filling the two columns, the peristaltic pump was used to saturate the residue with distilled water. Columns were then equilibrated for 48 hours prior to the commencement of leaching. Columns were leached with distilled water every two days in the first 60 days, at a pro-rata volume equivalent to that of the average annual rainfall in Guangxi (1800 mm), after which leaching was terminated and the columns were monitored for a further 270 days. Efflorescence appeared on the 90th day, and was sustained to the 150th day. After 150 days, efflorescence was difficult to observe. Hence, effloresced salts were sampled on the 150th day from columns C1 and C2. Fig.2 shows the daily air temperature and humidity averages in the laboratory from 0 to 100 days.

2.3 Analytical and statistical methods

During the leaching procedure, residues were collected at 0, 5, 15, 25, 35, 45, and 55 cm's depth on the 30th, 60th, 90th, 150th, 210th, 270th and 330th day with a spatula through each sampling hole (the 0 cm depth refers to the surface layer of the columns which sampled in the upper 0-1 cm). Three replicates were collected from different sampling holes which were positioned around the column at each sampling depth. Effloresced salts were removed by scraping them from the surface of the columns. The effloresced salt sample contained a small amount of bauxite residues from the surface layer (0-1cm depth) due to the small volume of material produced and the fact that the surface becomes cemented once the material is deposited. All samples were air-dried and then sieved to 0.84 mm (20 mesh) prior to analysis. The pH was

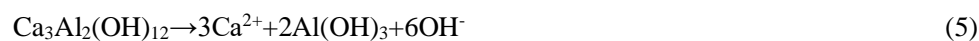
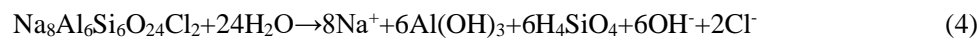
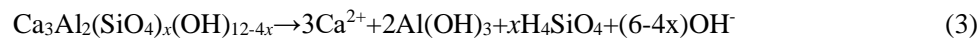
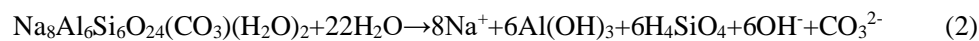
measured with an acidity meter (PHS-3C), and the solid-to-liquid ratio was m (solid):
v (liquid) = 1:5 (Kong et al., 2017a). Subsequent to pH determination, the supernatant
liquors were mixed at 150 rpm (1 h) then centrifuged at 3000 rpm (10 min) and
analyzed for CO_3^{2-} and HCO_3^- concentrations, which were determined by double
indicator-neutralization titration using H_2SO_4 (0.005 mol/L) (Kong et al.,
2017b). Aluminum concentrations and soluble concentrations of Na and Ca in all
prepared supernatants were determined by ICP-AES (Optima 5300DV inductively
coupled plasma spectrometer, Perkin Elmer) (Huang et al., 2016). Bauxite
residue/effloresced $\text{Al}(\text{OH})_4^-$ content was calculated by the Al concentrations in
supernatants. Air temperature and humidity were determined using a wet and dry
thermometer (HTC-1). Bulk density was determined on naturally compacted samples
using the cutting ring method, and moisture content was determined using the weight
method. Capillary porosity was calculated by multiplying the two together (Jones et
al., 2011). Particle morphologies and sizes were measured using SEM (FET
Quanta-200) and a laser scattering particle size analyzer (Malvern Mastersizer 2000
MS, UK). XRD for mineral identification was conducted on a Bruker D8 Discover
2500 with a $\text{Cu K}\alpha_1$ anode, using a Sol-X detector (LynxEye array). Near edge X-ray
absorption spectroscopy (NEXAFS) experiments were performed on the BL08U1A
beamline of the Shanghai Synchrotron Radiation Facility (SSRF, Shanghai, China).
Distribution of Na in the residual solids was analyzed by soft X-ray scanning
transmission microscopy (STXM); the specific determination method is detailed in
Kong et al. (2017b).

SPSS Statistics 24 software was used to analyze significant differences. The results of
test data are mean \pm standard deviation. Significant differences of the relative
parameters were statistically analyzed using significance F test and Duncan multiple
comparison method ($p < 0.05$ and $p < 0.01$). All figures were produced using Origin
V8.5 software.

3. Results and discussion

3.1 Efflorescence analysis

Efflorescence material on the surface of bauxite residue is closely related to the high alkaline species contained in the residue. The alkaline materials are commonly divided into two categories: free alkali and chemically bound alkali. Chemically bound alkali is produced in the process of pre-desilication, leaching and separation via a series of mineralization and chemical reactions. Due to its low solubility, good buffering performance and complex structure, it mainly exists in the form of mineral phases, including calcite (CaCO_3), cancrinite ($\text{Na}_8\text{Al}_6\text{Si}_6(\text{CO}_3)\text{O}_{24}\cdot 2\text{H}_2\text{O}$), hydrogarnet ($\text{Ca}_3\text{Al}_2(\text{SiO}_4)_x(\text{OH})_{12-4x}$), sodalite ($\text{Na}_8\text{Al}_6\text{Si}_6\text{O}_{24}\text{Cl}_2$), and tricalcium aluminate (TCA, $\text{Ca}_3\text{Al}_2(\text{OH})_{12}$). As revealed in dissolution equations 1 to 5, these mineral phases are capable of dissolving and generating OH^- and CO_3^{2-} under certain conditions (Xue et al., 2019b; Kong et al., 2017a). The other typical alkaline substances are free alkali, which mainly includes NaOH , Na_2CO_3 , NaHCO_3 , $\text{NaAl}(\text{OH})_4$, K_2CO_3 and KOH . The free alkali anions originate from dissolution of free alkali which form a strong buffer system to maintain the pH between 9.2 to 12.3.



Effloresced material harvested from column C1 was less than that from column C2. Therefore, material from C1 was only used for SEM, XRD and XANES analyses (see later sections). The change in typical alkaline anion content of soluble effloresced material in C2 is shown in Table 2 (it should be noted that time 0 day here refers to the upper 0-1 cm of pure bauxite residue). The pH of effloresced substances increased by nearly one unit, from 10.42 to 11.02. Two typical alkaline anions, CO_3^{2-} and HCO_3^- , present in soluble alkaline substances, increased their contents significantly from 141.3 and 31.28 mmol/L to 256.7 and 46.84 mmol/L respectively, indicating that they are still the main components of effloresced substances. Efflorescence continued to

occur in column C2 during the latter 90 to 150 days. The main period of efflorescence is typically 90-120 days, and alkaline anion content changes significantly, but with little change during the last 30 days. Total mass of effloresced salts in C2 column is relatively large, indicating that phosphogypsum influenced salt production. With time, water in C2 evaporated, halting the efflorescence process.

Fig. 3 shows the change in soluble cations (Na^+ and Ca^{2+}) in C2, which increased during the process of efflorescence. The main period of efflorescence occurred during the first 30 days, where Na^+ and Ca^{2+} concentrations changed greatly. In comparison to the original bauxite residue, Na^+ and Ca^{2+} ions increased from 76.34 and 3.12 mmol/L to 216.9 and 8.36 mmol/L respectively, indicating that sodium salt is the main soluble substance responsible for efflorescence production. That is, Na_2CO_3 and NaHCO_3 are the main soluble components in effloresced substances, this is consistent with the results of Klauber et al. (2013), which revealed efflorescence formation along with a changing phase composition in brine solids from sodium bicarbonate through to trona and then to carbonate monohydrate. In addition to the soluble effloresced salts, insoluble effloresced salts of CaCO_3 were found in C2 column, with the net reaction for this mechanism present in Eqs.6 (Burke et al., 2013; Lehoux et al., 2013).



3.2 pH and alkaline anion migration

pH in unamended bauxite residue (C1) decreased during the experiment, with pH values ranging from pH 9.76-11.02 (Fig. 4). Some variation in residue pH was observed with depth. Surface pH (0-1 cm depth) decreased from 0-60 days, then increased from 90-150 days, then decreased again from 120-330 days (Fig. 4). The increase in surface pH at 90-150 days coincides with efflorescence at this time, as discussed in Section 3.1, and likely reflects the dominance of alkali salts in the efflorescence. The largest decrease in residue pH occurred between 0-30 days, reflecting export of soluble alkaline substances in the bauxite residue to lower layers

of the soil column with the continuous migration of water, and eventual exit from the leaching column.

In the phosphogypsum-amended residue column (C2), residue pH was substantially lower in the upper 0-30 cm at time 0 (pH 8.5-9.5) than in the unamended residue column (C1; pH 10.7-11.0) (Fig. 4). The pH of phosphogypsum is low (approximately 2.5), and the addition of Ca^{2+} in phosphogypsum aids in pH neutralization through removal of OH^- and CO_3^{2-} from solution as $\text{Ca}(\text{OH})_2$ and CaCO_3 (Eqs.7, 8) (Li et al., 2018; Courtney and Timpson, 2004; Menzies et al., 2004; Suryavanshi et al., 1996; Paradis et al., 2007). As well as neutralizing residue pH, these reactions contributed to reducing efflorescence of sodium-based alkali salts at the surface during the drying phase of the experiment. Although some increases in surface (0-1 cm) pH of residue were observed in the C2 column at 90-150 days (pH at 60 days: 8.6; pH at 90 days: 9.21; pH at 150 days: 9.92), these were much lower than those observed in C1 (pH at 60 days: 10.1; pH at 90 days: 10.71; pH at 150 days: 11.02; Fig. 4). The results of pH changes with depth are similar to Bray et al. (2018).



Free alkali is an important contributor to bauxite residue alkalinity, including salts such as NaOH , Na_2CO_3 , NaHCO_3 , $\text{NaAl}(\text{OH})_4$, K_2CO_3 and KOH . These salts are readily dissolved to generate the alkaline anions OH^- , CO_3^{2-} , HCO_3^- , and $\text{Al}(\text{OH})_4^-$. We focused on concentrations of CO_3^{2-} and HCO_3^- in the bauxite residue as these dominate solution chemistry at the prevailing pH observed in the columns (Li et al., 2018). Trends in summed concentrations of CO_3^{2-} and HCO_3^- (termed as alkaline anion concentrations) in column C1 mirrored those of pH with depth and with time, decreasing overall during the experiment and with a substantial increase in surface concentrations coincident with efflorescence at 90-150 days (Fig. 4). This is consistent with water movement being the major control on migration of alkaline anions within unamended residue. Unlike C1, trends in summed concentrations of CO_3^{2-} and HCO_3^- in the phosphogypsum amended column C2 differed to those of pH.

Application of phosphogypsum in the upper 25 cm of residue substantially decreased alkaline anion concentrations at time zero, with alkaline anion concentrations in the 0-30 cm depths of <20 mmol/L in C2 compared to 235-270 mmol/L in C1 (Fig. 4). Alkaline anion concentrations then increased with depth (at time zero) in C2 to reach a maximum of 235 mmol/L at 55 cm (Fig. 4), like that of unamended residue in C1. As leaching proceeded over the first 60 days, alkaline anion concentrations decreased in the 30-60 cm depths of C2 which likely reflects both slow dissolution of phosphogypsum and reaction of Ca^{2+} with CO_3^{2-} and HCO_3^- in solution, as well as washout (export) of residual dissolved HCO_3^- and CO_3^{2-} from the leaching column (Fig. 4). At time 90 days and during the remainder of the experiment, alkaline anion concentrations were substantially lower in C2 (all < 80 mmol/L at all depths) than in C1 (205-305 mmol/L at all depths) (Fig. 4). As observed in C1, alkaline anion concentrations increased at the surface of C2 during the initial phase of drying (90-150 days), consistent with efflorescence of alkali salts.

After collecting the effloresced substances on the bauxite residue surface on the 150th day, pH and alkaline anion content of bauxite residue at all depths continued to show small decreases between the 210th and 330th days, but this range will become negligible over longer periods. Previous work revealed that repeated replacement of pore water does not alter the final pH, Na^+ , CO_3^{2-} , or OH^- contents due to the alkalinity released (Thornber and Binet, 1999).

3.3 Factors influencing efflorescence

The bauxite residue capillary porosity at different depths in C1 and C2 varied with time of 0-150 days (Fig.5a). The capillary porosity at different depths (0, 25, 45cm) in C1 column was basically unchanged, while the capillary porosity at 0, 25, 45cm in C2 column gradually increased with the extension of time, and there were significant differences between 30, 60, 90, 120 and 150 days and 0 days ($p < 0.05$). It indicates

that the addition of phosphogypsum can increase the capillary porosity of bauxite residue, which promotes the upward transportation of soluble salts. The moisture content of bauxite residue at different depths in C1 and C2 columns gradually decreased with the increases of time (Fig. 5b), especially when the leaching was suspended since the 60th days, the magnitude of reduction reached a maximum, and there were significant differences between the 90-150th days and 0-60th days ($p < 0.01$). The water in bauxite residue loss rapidly indicates that bauxite residue has a poor water retention ability, which has an adverse effect on the efflorescence, because the majority of soluble salts are transported to the surface of bauxite residue by water migration, thus causing spontaneous efflorescence formation.

The Fig.5c showed the comparison of the particle size of the bauxite residue (sampled at the end of experiments of day 330) at 25 cm and 45 cm depth in column C1 and C2. It illustrated that the particle size changed little between the depth of 25 and 45 cm column C1, whilst compared to the correspondingly same depth in column C2, the volume fraction of particle size range in 0.1-1 μ m increased from 0.5 to 1.5%, and that of 100-1000 μ m increased from 1 to 3.3%. It indicates that the particle size of bauxite residue in C2 column increases with the increase of depth, which is related to the application of phosphogypsum. Previous studies have proved that phosphogypsum can promote the formation of large aggregates of bauxite residue (Xue et al., 2019). The increase of particle size of bauxite residue also means that getting more porosities between bauxite residue particles, which is conducive to the migration of water to the surface and promotes the efflorescence forming at the surface of bauxite residue to some extent (Zhu et al., 2016).

3.4 Mineralogy and morphology of effloresced salts

The samples of the surface efflorescence substances (0-1 cm) and the bauxite residue at 45 cm depth were selected to analyze the mineral phase composition (Fig.6). Hematite (Fe_2O_3) is a major mineral component of bauxite residue, with calcite

(CaCO_3), tricalcium aluminate ($\text{Ca}_3\text{Al}_2(\text{OH})_{12}$), cancrinite ($\text{Na}_8\text{Al}_6\text{Si}_6\text{O}_{24}(\text{CO}_3)(\text{H}_2\text{O})_2$) and hydrogarnet ($\text{Ca}_3\text{Al}_2(\text{SiO}_4)_x(\text{OH})_{12-4x}$) as the main alkaline mineral phases in both C1 and C2 (Fig. 6). The five minerals in the bauxite residue persist in C1 and C2 throughout the trials, as observed in the similarity in XRD patterns collected from both columns at 45 cm depth below surface at day 150. The surface 0-1 cm samples in both C1 and C2 were dominated by effloresced salts, chiefly sodium sulfate ($\text{Na}_2\text{SO}_4 \cdot 10\text{H}_2\text{O}$). This reflects the dominance of Na^+ and SO_4^{2-} in bauxite residue pore water wt.% (Santini et al., 2011; Santini and Fey, 2012), which are brought to the surface by capillary rise. A large peak of sodium sulfate ($\text{Na}_2\text{SO}_4 \cdot 10\text{H}_2\text{O}$) appears in the mineral phase of the surface efflorescence sample, the peak strength of calcite also decreased significantly while the peak of hydrogarnet and cancrinite disappeared.

As visible in the sample at 45 cm in C1 column (Fig. 7b), the unamended bauxite residue showed morphology dominated by loose, rounded and platy particles varying in size from approximately 50 to 500 nm in diameter. The morphology of bauxite residue above which phosphogypsum had been applied (Fig. 7d; 45 cm depth in C2) showed some agglomerations of the smaller particles visible in Fig. 7b into larger aggregates, with an absence of platy particles. This may be due to the effect of added phosphogypsum precipitating out excess Ca^{2+} as CaCO_3 which cemented smaller particles together. The surface efflorescence samples of C1 and C2 columns (Fig. 7a/c) showed smooth, platy (and occasionally acicular in C1, and occasionally fibrous in C2) particles of diameters 100-500 nm. Electron microprobe analysis of effloresced salts from C1 and C2 confirmed substantially higher concentrations of sodium in these salts (C1: 12.78 wt.%; C2: 30.92 wt.%) than in the bulk residue (C1: 3.28 wt.%; C2: 5.52 wt.%), consistent with XRD results reported above showing a dominance of $\text{Na}_2\text{SO}_4 \cdot 10\text{H}_2\text{O}$ in the effloresced salts. Surface treatment with phosphogypsum can promote the formation of stable macroaggregates to form new particles and accelerate the occurrence of efflorescence forming at the surface of bauxite residue. Another study has reported that phosphogypsum changed the microstructure and surrounding pores of residue aggregates (Xue et al., 2020). Therefore, selecting the appropriate

way to transform the efflorescence substances can not only effectively reduce the alkalinity of bauxite residue, but also promote the soil formation process of bauxite residue.

3.5 Phase equilibrium diagram of Na_2CO_3 and Na_2SO_4

Of particular interest in this efflorescence process are the mechanisms causing the phase transformations in effloresced salts as well as the mechanisms by which the salts are brought to the surface through capillary rise. A key factor in both appears to be the Na_2CO_3 and Na_2SO_4 chemistry. The solubility of the Na_2CO_3 and Na_2SO_4 salt-water system were studied at 0 to 100 °C by isothermal method, and the corresponding equilibrium diagram was plotted (Fig. 8). The phase equilibrium of salt-water system was affected by temperature. The Fig. 8a shows sodium bicarbonate, trona and sodium carbonate monocarbonate at low temperature (reprinted from Klauber et al., 2013). The main solid phase component in liquid in the range of 20-40 °C was NaHCO_3 . Water loss from the residue, especially at the surface, drives the transformation of NaHCO_3 into sodium carbonate monohydrate being consistent with results discussed in section 3.1.

The diagram shows the phase diagram of Na_2SO_4 -water binary system at low temperature (Fig. 8b) (redrawn from Niu et al., 2002). In column C2, due to the addition of phosphogypsum, Eqs. 6 above shows that the generated sulfate ions react with a large number of free sodium ions in bauxite residue to produce sodium sulfate. In a binary water and salt system, Na_2SO_4 will form a stable hydrated salt of $\text{Na}_2\text{SO}_4 \cdot 10\text{H}_2\text{O}$ with water at low temperature. The $\text{Na}_2\text{SO}_4 \cdot 10\text{H}_2\text{O}$ is then converted into Na_2SO_4 at 32.38 °C, through dehydration. Therefore, amorphous Na_2SO_4 will be transformed into $\text{Na}_2\text{SO}_4 \cdot 10\text{H}_2\text{O}$ having a crystal structure through phase transformation. Its characteristic peak was observed with XRD determination (detailed in section 3.4). To conclude, the phase equilibrium diagram of Na_2CO_3 and Na_2SO_4 showed variation in composition of the effloresced material. In C1 it is

mainly sodium carbonate, which is strongly alkaline, while in C2 it is mainly sodium sulfate (neutral salt) mixed with a small amount of sodium carbonate and sodium bicarbonate. Therefore, carbonate and bicarbonate in C2 is slightly less than that in C1, and its pH value is slightly lower than that of C1. This is also why the pH value of the effloresced material in C2 does not change much with time, and the alkaline anion concentrations of carbonate and bicarbonate do not change much in the later period of the investigation. Simultaneously, it also demonstrates that addition of phosphogypsum changes the composition of alkaline effloresced materials, and converts some of them into neutral salts with higher molar mass, which alleviates alkaline dust production to the surrounding environment but promotes the amounts of efflorescence.

3.6 XANES spectrum analysis

The Na K-edge X-ray absorption near edge structure (XANES) spectra (Fig.9a) collected from the surface (0 cm) and 45 cm deep have been normalized. The XANES spectra have two obvious feature absorption peaks a and b. C1 surface feature absorption peak a (location: 1067.0 ± 0.2 eV, normalized intensity: 0.073) and feature absorption peak b (location: 1071.0 ± 0.2 eV, normalized intensity: 0.072); 45 cm feature absorption peak a (position: 1067.0 ± 0.2 eV, normalized intensity: 0.060) and feature absorption peak b (position: 1071.0 ± 0.2 eV, normalized intensity: 0.058); C2 surface feature absorption peak a (position: 1068 ± 0.2 eV, normalized strength: 0.098) and feature absorption peak b (position: 1071.0 ± 0.2 eV, normalized strength: 0.100); 45 cm feature absorption peak a (position: 1068.0 ± 0.2 eV, normalized intensity: 0.084) and feature absorption peak b (position: 1071.0 ± 0.2 eV, normalized intensity: 0.085). The XANES spectra for reference materials were obtained from cancrinite (adsorption peaks of b and e, located at 1067.5 and 1072.0 eV, normalized intensities of 0.068 and 0.072). XANES analysis of Na K-edge indicated that two prominent absorption peaks b and e, from C2-0 and C2-45 residues, were almost uniform and similar to the cancrinite spectrum except for the C1-0 and C1-45 residues. The local ordering

around Na (Na is in a tetrahedral position surrounded by one CO₃ at 2.701 Å and three O at 2.398 Å in a trigonal pyramid) did not change (Neuville et al., 2004). This indicated that phosphogypsum had no effect on the phase transformation of cancrinite in bauxite residue.

The sodium STXM imaging of 0 and 45 cm depth in C1 and C2 are presented in Fig. 9b. The X-ray absorption images of 0 and 45 cm depth bauxite residue in C1 at the spatial resolution of 30-50 nm (spatial distribution of mesoporous scale) are shown in Fig. 9 (C1-0 and C1-45). The spatial distribution of Na in the surface layer is relatively dense (the darker the color, the more Na content) (Kong et al., 2017b). The distribution is sparse at a depth of 45 cm, the spatial distribution of Na in the surface layer is relatively concentrated, and Na at 45cm is uniformly dispersed. The X-ray absorption images of 0 and 45 cm depth in C2, at spatial resolution of 30-50 nm (spatial distribution of mesoporous scale), are presented in Fig. 9 (C2-0 and C2-45). Sodium was densely distributed in space at the surface layer and sparsely distributed at depth (45cm). Both C1 and C2 showed that Na was densely distributed in the surface layer, and Na distribution was sparser with an increase in depth. The mesoporous scale spatial distribution of Na in bauxite residue (C2) at the surface and 45cm depth, was denser than that of the original bauxite residue (C1). The mesoporous scale spatial distribution of Na in bauxite residue was changed by phosphogypsum, and the effect on the bauxite residue surface was more apparent. Using NEXAFS analysis, Kong et al. (2017b) found that acid treatment and gypsum combination had no effect on Na speciation but affected its distribution. The spatial distribution of Na further indicated that phosphogypsum treatment lead to dissolve more alkaline minerals and changed the chemical form of Na minerals in the residue.

4. Conclusions

This work has revealed that effloresced materials on the surface of bauxite residue are formed through the migration of soluble alkaline ions along with water. During the

first 150 days, CO_3^{2-} and HCO_3^- respectively increased from 141.3 and 31.28 mmol/L to 256.7 and 46.84 mmol/L, and Na^+ and Ca^{2+} increased from 76.34 and 3.12 mmol/L to 216.9 and 8.36 mmol/L, respectively. Sodium salts are the main soluble substances formed. During the leaching process, pH and free alkali decreased in surface residue (0-15 cm). The efflorescence phenomenon began to appear gradually during 90-150 days and pH and free alkali content in C2 increased from 8.68 and 8.44 mmol/L at the surface, to 9.21 and 8.56 mmol/L at 55 cm depth, respectively. The key factors for dust formation at conventional BRDAs are particle size, capillary porosity and moisture content during the efflorescence process. The solid phase transformation of sodium carbonate and sodium sulfate in C1 and C2 explains the conversion of efflorescence materials in bauxite residue (sodium carbonate - sodium bicarbonate; sodium sulfate - sodium sulfate crystal water). XANES spectra revealed the spatial distribution of Na on the surface of C1 and C2 which was relatively concentrated, whilst Na was uniformly dispersed at 45 cm, and Na distribution became sparser with an increase in depth. Phosphogypsum reduces the occurrence of alkaline efflorescence efficiently. More significantly, these findings are beneficial in order to eliminate environmental risk of alkaline dust pollution and have an important implication for the phosphogypsum used as a common amendment application in rehabilitation on BRDAs in the future.

Declaration of Competing Interest

The authors declare that they have no known competing financial interests or personal relationships that could have appeared to influence the work reported in this paper.

Acknowledgments

This work was supported by the National Key Research and Development Program of China (No. 2019YFC1803605); and the National Natural Science Foundation of China (No. 41877511).

References

495 Bray, A.W., Stewart, D.I., Courtney, R., Rout, S.P., Humphreys, P.N., Mayes, W.M., Burke, I.T.,
 496 2018. Sustained Bauxite Residue Rehabilitation with Gypsum and Organic Matter 16 years after
 497 Initial Treatment. *Environ. Sci. Technol.* 52, 152-161.

498 Burke, I.T., Peacock, C.L., Lockwood, C.L., Stewart, D.I., Mortimer, R.J.G., Ward, M.B.,
 499 Renforth, P., Gruiz, K., Mayes, W.M., 2013. Behavior of Aluminum, Arsenic, and Vanadium
 500 during the Neutralization of Red Mud Leachate by HCl, Gypsum, or Seawater. *Environ. Sci.*
 501 *Technol.* 47, 6527-6535.

502 Collins, R.N., Clark, M.W., Payne, T.E., 2014. Solid phases responsible for Mn^{II} , Cr^{III} , Co^{II} , Ni,
 503 Cu^{II} and Zn immobilization by a modified bauxite refinery residue (red mud) at pH 7.5. *Chem.*
 504 *Eng. J.* 236, 419-429.

505 Courtney, R., Timpson, J.P., 2004. Nutrient status of vegetation grown in alkaline bauxite
 506 processing residue amended with gypsum and thermally dried sewage sludge - A two year field
 507 study. *Plant Soil.* 266, 187-194.

508 Courtney, R., Harrington, T., 2012. Growth and nutrition of *Holcus lanatus* in bauxite residue
 509 amended with combinations of spent mushroom compost and gypsum. *Land Degrad. Dev.* 23,
 510 144-149.

511 Courtney, R., Feeney, E., O'Grady, A., 2014. An ecological assessment of rehabilitated bauxite
 512 residue. *Ecol. Eng.* 73, 373-379.

513 Courtney, R., Xue, S.G., 2019. Rehabilitation of bauxite residue to support soil development and
 514 grassland establishment. *J. Cent. South Univ.* 26, 353-360.

515 Ding, X.H., Xu, G., Liu, W.V., Yang, L., Albijanic, B., 2019. Effect of polymer stabilizers'
 516 viscosity on red sand structure strength and dust pollution resistance. *Powder Technol.* 352,
 517 117-125.

518 Gelencser, A., Kovats, N., Turoczi, B., Rostasi, A., Hoffer, A., Imre, K., Nyiro-Kosa, I.,
 519 Csakberenyi-Malasics, D., Toth, A., Czitrovsky, A., Nagy, A., Nagy, S., Acs, A., Kovacs, A.,
 520 Ferincz, A., Hartyani, Z., Posfai, M., 2011. The Red Mud Accident in Ajka (Hungary):
 521 Characterization and Potential Health Effects of Fugitive Dust. *Environ. Sci. Technol.* 45,
 522 1608-1615.

523 Gomes, H.I., Mayes, W.M., Rogerson, M., Stewart, D.I., Burke, I.T., 2016. Alkaline residues and
 524 the environment: a review of impacts, management practices and opportunities. *J. Clean. Prod.*

112, 3571-3582.

Grafe, M., Power, G., Klauber, C., 2011. Bauxite residue issues: III. Alkalinity and associated chemistry. *Hydrometallurgy*. 108, 60-79.

Higgins, D., Curtin, T., Burke, I., Courtney, R., 2018. The potential for constructed wetland mechanisms to treat alkaline bauxite residue leachate: carbonation and precipitate characterization. *Environ. Sci. Pollut. R.* 25, 29451-29458.

Hong, S.Y., Glasser, F.P., 2002. Alkali sorption by C-S-H and C-A-S-H gels: Part II. Role of alumina. *Cement. Concrete Res.* 32, 1101-1111.

Huang, J., Lin, L., Yu, Y.J., Lan, M.Z., Zhang, J.S., Gao, D.F., Wang, X.T., Yang, J.B., 2014. Technical and Product Evaluation of Industrial Solid Waste. China Standard Press, Beijing, 2014.

Huang, Y.F., Chai, W.C., Han, G.H., Wang, W.J., Yang, S.Z., Liu, J.T., 2016. A perspective of stepwise utilisation of Bayer red mud: Step two-Extracting and recovering Ti from Ti-enriched tailing with acid leaching and precipitate flotation. *J. Hazard. Mater.* 307, 318–327.

Indraratna, B., Athukorala, R., Vinod, J., 2013. Estimating the rate of erosion of a silty sand treated with lignosulfonate. *J. Geotech. Geoenviron.* 139, 701-714.

Johnston, M., Clark, M.W., McMahon, P., Ward, N., 2010. Alkalinity conversion of bauxite refinery residues by neutralization. *J. Hazard. Mater.* 182, 710-715.

Jones, B.E.H., Haynes, R.J., Phillips, I.R., 2011. Influence of organic waste and residue mud additions on chemical, physical and microbial properties of bauxite residue sand. *Environ. Sci. Pollut. R.* 18, 199-211.

Khaitan, S., Dzombak, D.A., Lowry, G.V., 2009. Chemistry of the acid neutralization capacity of bauxite residue. *Environ. Eng. Sci.* 26, 873-881.

Klauber, C., Harwood, N., Hockridge, R., Middleton, C., 2013. Proposed Mechanism for the Formation of Dust Horizons on Bauxite Residue Disposal Areas. *Essential Readings in Light Metals: Alumina and bauxite*, first ed. John Wiley & Sons Inc, New Jersey.

Kong, X.F., Guo, Y., Xue, S.G., Hartley, W., Wu, C., Ye, Y.Z., Cheng, Q.Y., 2017a. Natural evolution of alkaline characteristics in bauxite residue. *J. Clean. Prod.* 143, 224-230.

Kong, X.F., Li, M., Xue, S.G., Hartley, W., Chen, C.R., Wu, C., Li, X.F., Li, Y.W., 2017b. Acid transformation of bauxite residue: conversion of its alkaline characteristics. *J. Hazard. Mater.* 324, 382-390.

555 Lehoux, A.P., Lockwood, C.L., Mayes, W.M., Stewart, D.I., Mortimer, R.J., Gruiz, K., Burke, I.T.,
 556 2013. Gypsum addition to soils contaminated by red mud: implications for aluminium, arsenic,
 557 molybdenum and vanadium solubility. *Environ. Geochem. Hlth.* 35, 643-656.

558 Li, X.F., Ye, Y.Z., Xue, S.G., Wu, C., Kong, X.F., Hartley, W., Li, Y.W., 2018. Leaching
 559 optimization and dissolution behavior of alkaline anion in bauxite residue. *T. Nonferr. Metal. Soc.*
 560 06, 1248-1255.

561 Li, X.F., Guo, Y., Zhu, F., Huang, L.B., Hartley, W., Li, Y.W., Kong, X.F., Xue, S.G., 2019.
 562 Alkalinity stabilization behavior of bauxite residue: Ca-driving regulation characteristics of
 563 gypsum. *J. Cent. South Univ.* 26, 383-392.

564 Liu, W.C., Yang, J.K., Xiao, B., 2009. Application of Bayer red mud for iron recovery and
 565 building material production from aluminosilicate residues. *J. Hazard. Mater.* 161, 474-478.

566 Luo, M.X., Qi, X.J., Zhang, Y.R., Ren, Y.F., Tong, J.C., Chen, Z.N., Hou, Y.M., Yeerkebai, N.,
 567 Wang, H.T., Feng, S.J., Li, F.T., 2017. Study on dealkalization and settling performance of red
 568 mud. *Environ. Sci. Pollut. R.* 24, 1-9.

569 Menzies, N., Fulton, I.M., Morrell, W.J., 2004. Seawater Neutralization of Alkaline Bauxite
 570 Residue and Implications for Revegetation. *J. Environ. Qual.* 33, 1877-1884.

571 Mishra, B., Staley, A., Kirkpatrick, D., 2002. Recovery of value-added products from red mud.
 572 *Min. Metall. Explor.* 19, 87-94.

573 Neuville, D.R., Cormier, L., Flank, M.A., Prado, R.J., Lagarde, P., 2004. Na K-edge XANES
 574 spectra of minerals and glasses. *Eur. J. Mineral.* 16, 809–816.

575 Niu, Z.D., Cheng, F.Q., 2002. Phase diagram of water and salt system and its application. Tianjin
 576 university press, Tianjin. (in Chinese)

577 Paradis, M., Duchesne, J., Lamontagne, A., Isabel, D., 2007. Long-term neutralisation potential of
 578 red mud bauxite with brine amendment for the neutralisation of acidic mine tailings. *Appl.*
 579 *Geochem.* 22, 2326-2333.

580 Rollings, R.S., Burkes, J.P., Rollings, M.P., 1999. Sulfate attack on cement-stabilized sand. *J.*
 581 *Geotech. Geoenviron.* 125, 364-372.

582 Suryavanshi, A.K., Scantlebury, J.D., Lyon, S.B., 1996. Mechanism of Friedel's salt formation in
 583 cements rich in tri-calcium aluminate. *Cement. Concrete Res.* 26, 717-727.

584 Santini, T.C., Hinz, C., Rate, A.W., Gilkes, R.J., Carter, C.M., 2011. In situ neutralization of

uncarbonated bauxite residue mud by cross layer leaching with carbonated bauxite residue mud. J. Hazard. Mater. 194, 119-127.

Santini, T.C., Fey, M.V., 2012. Synthesis of hydrotalcite by neutralization of bauxite residue mud leachate with acidic saline drainage water. Appl. Clay Sci. 55, 94-99.

Santini, T.C., Kerr, J.L., Warren, L.A., 2015. Microbially-driven strategies for bioremediation of bauxite residue. J. Hazard. Mater. 293, 131-157.

Santini, T.C., Peng, Y.G., 2017. Microbial fermentation of organic carbon substrates drives rapid pH neutralisation and element removal in alkaline bauxite residue leachate. Environ. Sci. Technol. 51, 12592-12601.

Sharma, J.V., Lhouvum, G., Chauhan, S., Lal, B., Singh, T.P., Paul, V., 2004. Rehabilitation of red mud ponds at INDAL, Belgaum (Karnataka). Indian Forester. 130, 481-497.

Shi, B., Qu, Y., Li, H., 2017. Gypsum alleviated hydroxyl radical-mediated oxidative damages caused by alkaline bauxite residue in leaves of *Atriplex canescens*. Ecol. Eng. 98, 166-171.

Smiciklas, I., Smiljanic, S., Peric-Grujic, A., Sljivic-Ivanovic, M., Mitric, M., Antonovic, D., 2014. Effect of acid treatment on red mud properties with implication on Ni (II) sorption and stability. Chem. Eng. J. 242, 27-35.

Sofra, F., Boger, D.V., 2002. Environmental rheology for waste minimisation in the minerals industry. Chem. Eng. J. 86, 319-330.

Thornber, M., Binet, D., 1999. Caustic Soda Adsorption on Bayer Residues. In 5th International Alumina Quality Workshop; AQW Inc. Bunbury, 498–507.

Vinod, J.S., Indraratna, B., Mahamud, M., 2010. Stabilisation of an erodible soil using a chemical admixture. P. ICE.-Ground Improvement. 163, 43-51.

Wang, Y.X., Zhang, T.A., Lyu, G.Z., Guo, F.F., Zhang, W.G., Zhang, Y.H., 2018. Recovery of alkali and alumina from bauxite residue (red mud) and complete reuse of the treated residue. J. Clean. Prod. 188, 456-465.

Wen, Z., Ma, S., Zheng, S., Zhang, Y., Liang, Y., 2016. Assessment of environmental risk for red mud storage facility in China: a case study in Shandong Province. Environ. Sci. Pollut. R. 23, 11193–11208.

Wieslawa, N.W., 1999. Effect of Na and Al on the phase composition and morphology of autoclaved calcium silicate hydrates. Cement. Concrete Res. 29, 1759-1767.

615 Xu, G., Ding, X.H., Kuruppu, M., Zhou, W., Biswas, W., 2018. Research and application of
616 non-traditional chemical stabilizers on bauxite residue (red sand) dust control, a review. *Sci. Total.*
617 *Environ.* 616-617, 1552-1565.

618 Xue, S.G., Zhu, F., Kong, X.F., Wu, C., Huang, L., Huang, N., Hartley, W., 2016. A review of the
619 characterization and revegetation of bauxite residues (Red mud). *Environ. Sci. Pollut. R.* 23,
620 1120-1132.

621 Xue, S.G., Li, M., Jiang, J., Millar, G.J., Li, C.X., Kong, X.F., 2019b. Phosphogypsum
622 stabilization of bauxite residue: Conversion of its alkaline characteristics. *J. Environ. Sci.-China.*
623 77, 1-10.

624 Xue, S.G., Wu, Y.J., Li, Y.W., Kong, X.F., Zhu, F., William, H., Li, X.F., Ye, Y.Z., 2019a.
625 Industrial wastes applications for alkalinity regulation in bauxite residue: A comprehensive review.
626 *J. Cent. South Univ.* 26, 268-288.

627 Xue, S.G., Ke, W.S., Zhu, F., Ye, Y.Z., Liu, Z., Fan, J.R., Hartley, W., 2020. Effect of
628 phosphogypsum and poultry manure on aggregate-associated alkaline characteristics in bauxite
629 residue. *J. Environ. Manage.* 256, 109981.

630 Yoon, K., Cho, D.W., Tsang, Y.F., Tsang, D.C.W., Kwon, E.E., Song, H., 2019. Synthesis of
631 functionalised biochar using red mud, lignin, and carbon dioxide as raw materials. *Chem. Eng. J.*
632 361, 1597-1604.

633 Zhu, F., Xue, S.G., Hartley, W., Huang, L., Wu, C., Li, X.F., 2016. Novel predictors of soil genesis
634 following natural weathering processes of bauxite residues. *Environ. Sci. Pollut. R.* 23,
635 2856-2863.

636 Zhu, F., Hou, J.T., Xue, S.G., Wu, C., Wang, Q.L., Hartley, W., 2017. Vermicompost and gypsum
637 amendments improve aggregate formation in bauxite residue. *Land Degrad. Dev.* 28, 2109-2120.